Thermodynamics of spin-orbit-coupled bosons in two dimensions from the complex Langevin method

Felipe Attanasio [*]

Department of Physics, University of Washington, Box 351560, Seattle, Washington 98195-1560, USA

Joaquín E. Drut[†]

Department of Physics and Astronomy, University of North Carolina, Chapel Hill, North Carolina 27599-3255, USA

We investigate the thermal properties of interacting spin-orbit-coupled bosons with contact interactions in two spatial dimensions. To that end, we implement the complex Langevin method, motivated by the appearance of a sign problem, on a square lattice with periodic boundary conditions. We calculate the density equation of state nonperturbatively in a range of spin-orbit couplings and chemical potentials. Our results show that mean-field solutions tend to underestimate the average density, especially for stronger values of the spin-orbit coupling. Additionally, the finite nature of the simulation volume induces the formation of pseudocondensates. These have been observed to be destroyed by the spin-orbit interactions.

I. INTRODUCTION

The experimental realization of ultracold atomic systems with spin-orbit coupling (SOC), nearly a decade ago [1–3], opened an exciting new set of directions for the exploration of the properties of matter in extreme (yet highly controllable) conditions. The SOC, which couples the atomic pseudospin (which itself denotes the particle species or "flavor") to momentum, is realized as the coupling of conventional nonrelativistic neutral particles to a synthetic non-Abelian background gauge field [4–6]. Such a construction has potential applications for the exploration of a variety of physical situations (including Rashba- [7] and Dresselhaus-type [8] couplings). Notably, these systems have been under intense scrutiny in recent years as they may be used experimentally to realize exotic phases of matter such as supersolids [9–11] and superfluids with a crystalline structure, and study exotic topological properties [12–14].

More generally, ultracold bosons subject to SOC are known, at mean-field level, to exhibit stripe or plane wave phases [15,16]: the ground-state wave function in the former is composed of two plane waves propagating in opposite directions, leading to an interference pattern, while on the latter it has only one plane wave. Many recent studies have investigated mean-field properties of different types of SOC [17], and also first-order (one loop) quantum corrections [14,18]. Recent theoretical studies of spin-orbit coupling include its effect combined with finite angular momentum [19] and a harmonic trap [20]. As in other systems, characterizing the thermodynamics and phase transitions of SOC particles in a precise fashion requires nonperturbative approaches, such as Monte Carlo simulations, which take full account of quantum

and thermal effects. (Notably, Ref. [17] performed a classical Monte Carlo study, where thermal fluctuations were assumed to be much larger than quantum ones.)

In this work, we use a lattice Monte Carlo approach to characterize, in a nonperturbative fashion, some of the basic thermodynamic observables of SOC bosons with quartic interactions. Specifically, we use the complex Langevin method to study such a nonrelativistic Bose gas on a space-time lattice, determining the density equation of state, pressure, and pseudocondensate fraction. In our lattice formulation, the SOC interaction is compactified and appears as a constant background non-Abelian gauge field. This allows for an easy study of the limit of very large SOC compared to the momentum. We focus on two spatial dimensions, as that is the smallest number of dimensions in which a finite temperature phase transition is expected. Additionally, because we work in the grand-canonical ensemble, it is no more expensive to calculate with 100 particles than with 1 or 2, provided that finite-size effects are under control.

II. MODEL AND LATTICE FORMULATION

We consider a system of $(2+1)$-dimensional nonrelativistic bosons with two hyperfine (pseudospin) states, denoted by $\uparrow$ and $\downarrow$, in Euclidean space-time. They are subject to a Rashba-Dresselhaus spin-orbit coupling (SOC) and density-density contact interactions. More specifically, we will use the Euclidean action

$$S = \int d^2x \, d\tau \, \mathcal{L}, \tag{1}$$

where $\mathcal{L} = \mathcal{L}_0 + \mathcal{L}_{\text{int}}$,

$$\mathcal{L}_0 = \Phi^\dagger(\partial_\tau - \mu)\Phi - \Phi^\dagger \frac{(-i\mathbb{1}\partial_x - \kappa_x\sigma_x)^2 + (-i\mathbb{1}\partial_y - \kappa_y\sigma_y)^2}{2m}\Phi, \tag{2}$$

*pyfelipe@uw.edu

†drut@email.unc.edu

is the free part, and

$$\mathcal{L}_{\text{int}} = \frac{\lambda}{4}[(\phi_\uparrow^\dagger \phi_\uparrow)^2 + (\phi_\downarrow^\dagger \phi_\downarrow)^2] + \frac{g}{2}(\phi_\uparrow^\dagger \phi_\uparrow \phi_\downarrow^\dagger \phi_\downarrow) \quad (3)$$

is the interacting part. In the above equations, $\Phi = [\phi_\uparrow \quad \phi_\downarrow]^T$, μ is the chemical potential for both species, m is the mass, λ and g are the intra- and interspecies couplings, and κ_x and κ_y characterize the spin-orbit interaction coupled to the σ_x and σ_y Pauli matrices. Note that, by virtue of the SOC, neither particle number is individually conserved, but the total particle number is, such that μ is a sensible chemical potential.

In order to perform our lattice studies, we discretize the system in a hypercubic lattice of size $N_x^2 \times N_\tau$ and spacings a and a_τ in the spatial and temporal directions, respectively. The temperature is given by $T = \beta^{-1} = 1/a_\tau N_\tau$. We assume periodic boundary conditions in all directions: this is necessary in the temporal direction for bosonic fields. The SOC enters the action in the same way as a background SU(2) gauge field, similar to a minimal coupling. On the lattice, the SOC is treated as a background non-Abelian gauge field and it is discretized in the same way [21,22]. The discretized version of the action, with the fields and couplings being rescaled by appropriate powers of the lattice spacing, is given by

$$S = \xi \sum_{\vec{x},\tau} \left\{ \Phi_{(\vec{x},\tau)}^\dagger \left(\Phi_{(\vec{x},\tau)} - e^{\xi\mu}\Phi_{(\vec{x},\tau-a_\tau)} \right) \xi^{-1} \right.$$
$$- \frac{1}{2m} \sum_j \Phi_{(\vec{x},\tau)}^\dagger \left[v_j \Phi_{(\vec{x}+a\hat{j},\tau)} + v_j^\dagger \Phi_{(\vec{x}-a\hat{j},\tau)} - 2\Phi_{(\vec{x},\tau)} \right]$$
$$\left. + \frac{\lambda+g}{8} \left(\Phi_{(\vec{x},\tau)}^\dagger \Phi_{(\vec{x},\tau-a_\tau)} \right)^2 + \frac{\lambda-g}{8} \left(\Phi_{(\vec{x},\tau)}^\dagger \sigma_z \Phi_{(\vec{x},\tau-a_\tau)} \right)^2 \right\},$$
$$(4)$$

where $\hat{j}$ represents a unit vector in the jth direction, $v_j = e^{-i\kappa_j \sigma_j}$, and $\xi = a_\tau/a$ is the lattice spacing anisotropy factor. The chemical potential has been introduced using the standard lattice formulation [23]. The contact interactions have been regularized in the same way as the number density operator. This formulation displays explicitly the global SU(2) flavor symmetry of the contact interactions when $\lambda = g$, and the conservation of the total particle number by all interactions due to the global U(1) symmetry.

In this work, we study the interplay between the self-coupling λ and the spin-orbit couplings κ_x and κ_y. The choice of $\lambda > g$ leads to, at mean-field level, a ground state described by a single plane wave [17], where we focus our studies for this work. We choose $g = 0$ for simplicity.[1] The coupling g between different pseudospins is left for a future publication.

Exact solution in the quadratic case

When the quartic terms are not present, the action (hereafter referred to as S_{free}) can be written in momentum

space as

$$S_{\text{free}} = \sum_{\vec{p},\omega} \tilde{\Phi}_{(\vec{p},\omega)}^\dagger M(\vec{p}, \omega, \mu, \vec{\kappa}) \tilde{\Phi}_{(\vec{p},\omega)}, \quad (5)$$

with

$$M = \begin{bmatrix} T + v_x^+ + v_x^- + v_y^+ + v_y^- & v_x^+ - v_x^- - i(v_y^+ - v_y^-) \\ v_x^+ - v_x^- + i(v_y^+ - v_y^-) & T + v_x^+ + v_x^- + v_y^+ + v_y^- \end{bmatrix}, \quad (6)$$

where $v_j^\pm = \xi \sin^2[(p_j \pm \kappa_j)/2]/m$ and $T = (1 - e^{\xi\mu}e^{i\omega_q})$. The lattice momenta and Matsubara frequencies are given by $p_j = 2\pi k_j/N_x$, with $k_j = 0, \ldots, N_x - 1$, and $\omega_q = 2\pi q/N_\tau$, with $q = 0, \ldots, N_\tau - 1$, respectively. The tildes represent Fourier transforms. The matrix M can be diagonalized via a change to the helicity basis:

$$\begin{bmatrix} \varphi_+ \\ \varphi_- \end{bmatrix} = \begin{bmatrix} \frac{(v_x^+ - v_x^-) + i(v_y^+ - v_y^-)}{\sqrt{2[(v_x^+ - v_x^-)^2 + (v_y^+ - v_y^-)^2]}} & \frac{1}{\sqrt{2}} \\ -\frac{(v_x^+ - v_x^-) + i(v_y^+ - v_y^-)}{\sqrt{2[(v_x^+ - v_x^-)^2 + (v_y^+ - v_y^-)^2]}} & \frac{1}{\sqrt{2}} \end{bmatrix} \begin{bmatrix} \phi_\uparrow \\ \phi_\downarrow \end{bmatrix}, \quad (7)$$

with eigenvalues

$$\lambda_\pm(\vec{p}, \omega, \mu, \vec{\kappa}) = T + v_x^+ + v_x^- + v_y^+ + v_y^-$$
$$\pm \sqrt{(v_x^+ - v_x^-)^2 + (v_y^+ - v_y^-)^2} \quad (8)$$

leading to the grand thermodynamic potential Ω via

$$\beta\Omega_{\text{free}}(\mu, \vec{\kappa}) = -\ln \mathcal{Z}_{\text{free}}$$
$$= \sum_{\vec{p},\omega} [\ln \lambda_+(\vec{p}, \omega, \mu, \vec{\kappa}) + \ln \lambda_-(\vec{p}, \omega, \mu, \vec{\kappa})]. \quad (9)$$

It is clear from the above equation that, since p_x and p_y run over the same interval, the free energy is symmetric under $\kappa_x \leftrightarrow \kappa_y$. Moreover, the partition function on the lattice is an even, periodic function of the spin-orbit couplings, with period π (in lattice units). This periodicity is a lattice artifact that disappears in the continuum limit.

The average density of the noninteracting case can be obtained by differentiation with respect to $\beta\mu$:

$$\langle n \rangle = \frac{1}{V} \frac{\partial \ln \mathcal{Z}}{\partial(\beta\mu)} = \sum_{s=\pm} \sum_{\vec{p},q} \frac{1}{1 - X_s(\vec{p}, \mu)e^{-i\omega_q}}, \quad (10)$$

where

$$X_s(\vec{p}, \mu) = e^{-\xi\mu}(1 + \lambda_s - T). \quad (11)$$

It can be shown that the sum over the Matsubara frequencies can be carried out, which yields

$$\langle n \rangle = \frac{1}{V} \sum_{s=\pm} \sum_{\vec{p}} \frac{1}{[X_s(\vec{p}, \mu)]^{N_\tau} - 1}. \quad (12)$$

In the $\xi \to 0$ limit,

$$[X_s(\vec{p}, \mu)]^{N_\tau} \to e^{\beta[\epsilon_s(\vec{p}, \vec{\kappa}) - \mu]}, \quad (13)$$

---

[1]Rotational properties of a similar system, but in three dimensions, have been studied in [19].

where, in the continuum limit,

$$
\epsilon_{\pm}(\vec{p}, \vec{\kappa}) = \frac{|\vec{p}|^2 + |\vec{\kappa}|^2}{2m}
$$
$$
\pm \frac{|\vec{p}||\vec{\kappa}|}{m} \sqrt{\cos^2(\theta_{\kappa})\cos^2(\theta_p) + \sin^2(\theta_{\kappa})\sin^2(\theta_p)},
$$
$$(14)$$

with $\theta_p = \tan^{-1}(p_y/p_x)$ and $\theta_{\kappa} = \tan^{-1}(\kappa_y/\kappa_x)$.

The continuum eigenvalues are given by

$$
\lambda_{\pm} = -i\omega - \mu + \epsilon_{\pm}(\vec{p}, \vec{\kappa}). \tag{15}
$$

Notice that, for $\omega = |\vec{\kappa}| = 0$, $\lambda_{\pm}$ vanishes at zero momentum and $\mu = 0$, signaling the well-known instability associated with Bose-Einstein condensation. For $|\vec{\kappa}| \neq 0$, the instability shifts to $\mu \neq 0$ and exists for both $|\vec{p}| = 0$ and $|\vec{p}| \neq 0$. The continuum eigenvalues have been studied in three dimensions in the Hamiltonian formulation for isotropic spin-orbit coupling in Ref. [24]. Additionally, one can see that $N_{\pm} = \varphi_{\pm}^{\dagger}\varphi_{\pm}$ are conserved and that $N_+ + N_- = N_{\uparrow} + N_{\downarrow}$.

Using trigonometric identities it is possible to show that $v_i^+ + v_i^- = \xi[1 - \cos(p_i)\cos(\kappa_i)]/m \to (p_i^2 + \kappa_i^2)/2m$ and $v_i^+ - v_i^- = \xi \sin(p_i)\sin(\kappa_i)/m \to p_i\kappa_i/m$. The arrows represent the behavior in the naive continuum limit. It is then clear that $\kappa_i = \pm\pi/2$ makes the p_i^2 term vanish on the lattice, corresponding to the limit where $|\kappa_i| \gg |p_i|$ in the continuum, such that the p_i^2 term can be ignored. When $|\vec{\kappa}| \gg |\vec{p}|$, such that the $|\vec{p}|^2$ term is negligible, the single particle Hamiltonian becomes an anisotropic Weyl Hamiltonian with $\vec{v}_0 = \vec{\kappa}/m$ playing the role of the (anisotropic) speed of light and an effective chemical potential of $-m|\vec{v}_0|^2/2$. A similar case has been discussed, in the context of ultracold fermionic atoms, in Ref. [25].

III. MANY-BODY METHOD

The first-order time derivative in the action is a non-Hermitian operator, making e^{-S} a complex weight for the path integral; this is known as phase (or sign) problem. This prevents the use of traditional Monte Carlo methods, since they use e^{-S} as a probability weight. One alternative in this scenario is the complex Langevin technique, which has been used to study theories with sign problems such as those with repulsive interactions [26] as well as polarized [27,28] and mass-imbalanced fermions [29] (see Ref. [30] for a review), finite density QCD with staggered quarks [31–34], random matrix models [35,36], rotating bosons [37,38], and superstring-inspired matrix models [39], among others.

The complex Langevin method is an extension of stochastic quantization [40]. The latter method consists of evolving the fields along a fictitious time dimension, θ, according to the Langevin equation

$$
\frac{\partial \phi_s(x, \tau)}{\partial \theta} = -\frac{\delta S}{\delta \phi_s(x, \tau)} + \eta_s(x, \tau), \tag{16}
$$

where $\eta_s(x, \tau)$ is a Gaussian white noise field satisfying

$$
\langle \eta_s(x, \tau) \rangle_{\eta} = 0, \tag{17}
$$

$$
\langle \eta_s(x, \tau)\eta_{s'}(x', \tau') \rangle_{\eta} = 2\delta(x - x')\delta(\tau - \tau')\delta_{ss'}, \tag{18}
$$

with $\langle \cdot \rangle_{\eta}$ indicating an ensemble average over the noise field. Quantum expectation values are obtained as

$$
\langle \hat{O} \rangle = \lim_{\theta \to \infty} \langle \hat{O}(\phi_{\uparrow}(\theta), \phi_{\downarrow}(\theta)) \rangle_{\eta}, \tag{19}
$$

where O is some observable. In practice, the Langevin equations are solved numerically with a step size $\varepsilon > 0$, chosen adaptively [41]. We follow a Euler-like discretization scheme in this work. This generates a sequence of field configurations. Ensemble averages are performed as simple averages of the observables calculated using the configurations generated after the system reaches its steady state.

In order to deal with theories that have a complex action, each of the fields has to be complexified [42–48]. For complex fields, both the real and imaginary parts become complex and obey the Langevin equation (16). We choose the noise to remain real [49]. Expectation values are calculated in the same way as in the case with real action. Note that real observables do become complex in this method, but their imaginary parts should be statistically compatible with zero.

In the complex Langevin method the fields obey a (Langevin-)time-dependent *real* probability distribution P defined on a complexification $\mathcal{M}_c$ of the original manifold $\mathcal{M}$. It can be shown that if the observables and action are holomorphic functions with sufficiently fast decay in the imaginary directions of $\mathcal{M}_c$, $\lim_{\theta \to \infty} P \propto e^{-S}$, which is the weight on the path integral (for a more detailed description, see [48,49]). Effects of slow decay in the imaginary directions have been studied in [50,51].

The average density was calculated as

$$
\langle n \rangle = \frac{1}{V} \frac{\partial \ln \mathcal{Z}}{\partial(\beta\mu)} = \frac{1}{V} \sum_{x,\tau} \langle n_{x,\tau} \rangle
$$
$$
= \frac{e^{\xi\mu}}{V} \sum_{x,\tau} \langle \Phi_{(x,\tau)}^{\dagger} \Phi_{(x,\tau-a_{\tau})} \rangle, \tag{20}
$$

where the angular brackets on the right-hand side indicate an average over configurations generated by the Langevin process. Mean-field results can be obtained by solving the Langevin equation without noise, which finds the minimum of the action.

We have performed our simulations on a periodic lattice of volume $20^2 \times 64$, a spacing anisotropy of $\xi = 1/8$, and mass $m = 1$. These parameters lead to a thermal wavelength of ~ 7 in lattice units, which is consistent with the continuum limit window $1 \ll \lambda_T/a \ll N_x$. This also guarantees that effects due to the choice of boundary conditions should be small. The Langevin step size was chosen adaptively, with an average of $O(10^{-4})$. We have estimated the autocorrelation time via the method proposed in [52]. The error bars shown in our plots represent statistical errors.

IV. RESULTS

A. Quadratic case

We have studied the case of noninteracting ($\lambda = 0$) exactly on the lattice. The average particle number density can be seen in Fig. 1. One can see that the density has its minimum when the system becomes Weyl-like, i.e., when the p^2 term in the Hamiltonian is much smaller than $\vec{\sigma} \cdot \vec{p}$ and can be neglected.
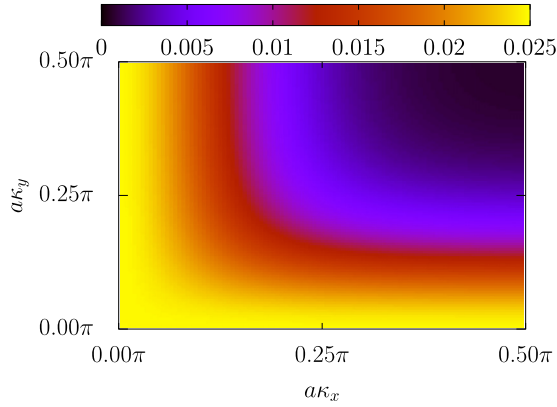
FIG. 1. Average particle number density, in units of the spatial lattice spacing a, as a function of the spin-orbit couplings at $\lambda = 0$. The simulations were performed at $\beta\mu = -0.8$.

At $\beta\mu \geqslant 0$ and $\kappa_x = \kappa_y = 0$ the condensation of bosons in the ground state makes the simulation unstable. This condensation is sharper at $T = 0$ and softer at $T > 0$, which is our case. For nonzero spin-orbit couplings, however, the chemical potential where such condensation happens is pushed to larger values due to the κ^2 term behaving as an effective chemical potential. To better visualize this, we have calculated the average density as a function of κ_x and κ_y by including only their effect on the chemical potential, i.e., the terms proportional to $\cos(\kappa_j)$, and ignoring the $\sin(\kappa_j)$ terms ($\vec{\sigma} \cdot \vec{p}$ in the continuum). The result is shown in Fig. 2. The figure further shows that the $\vec{\sigma} \cdot \vec{p}$ term in the continuum action has a nontrivial effect on the average density.

B. Interacting case I—isotropic SOC

As an initial check on the ability of the complex Langevin method to give correct results, we have looked at the imaginary part of the density. Despite the sign problem in the Euclidean formulation, the density is expected to be (statistically compatible with) zero. This can be verified in Fig. 3.
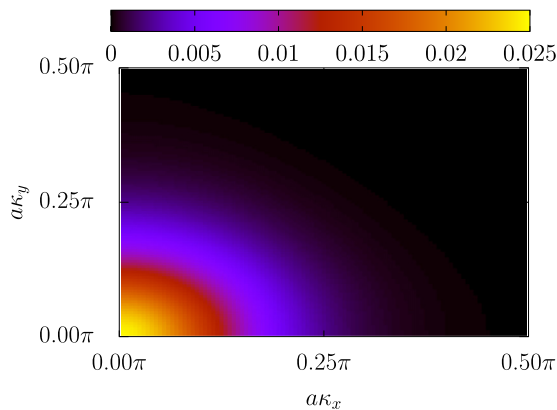

FIG. 2. Average particle number density, in units of the spatial lattice spacing a, as a function of the spin-orbit couplings at $\lambda = 0$ and ignoring the $\sin(\kappa_j)$ terms. The simulations were performed at $\beta\mu = -0.8$.
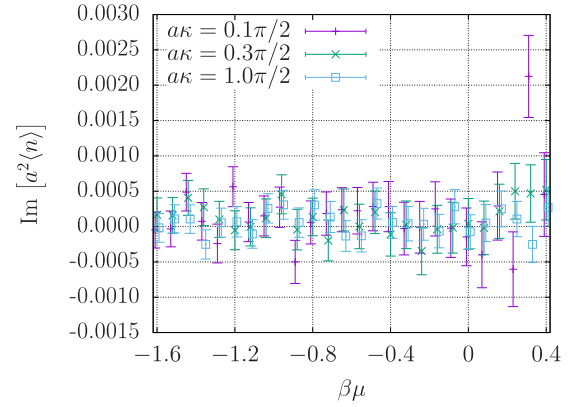

FIG. 3. Imaginary part of the average density, in units of the spatial lattice spacing a, as a function of $\beta\mu$ for different values of the spin-orbit coupling. We have considered an interaction between particles of the same pseudospin, with coupling $\lambda/a = 0.5$. Points have been slightly shifted horizontally for clarity.

Throughout this section we have used $\kappa_x = \kappa_y \equiv \kappa$. Complex-valued densities would indicate a failure of the simulations.

The repulsive quartic couplings, similar to the spin-orbit couplings, have the effect of keeping the system stable at small but positive chemical potentials. This can be seen in Fig. 4, where we show the average density as a function of $\beta\mu$ for different values of (isotropic) SOC at $\lambda/a = 0.5$. As in the case of $\lambda = 0$, indicated by the long-dashed, short-dashed, dotted, and dash-dotted lines for each κ, we observe smaller densities as the spin-orbit coupling increases.

The mean-field average density is also shown in the figure. For each flavor, it is given by

$$\langle n_s \rangle = \frac{2e^{\xi\mu}\{e^{\xi\mu} - 1 - \xi/m[\cos(\kappa_x) + \cos(\kappa_y) - 2]\}}{\xi\lambda} \quad (21)$$

and is zero when the right-hand side is negative. For the larger values of κ shown in the figure, the mean-field density becomes positive at much higher values of $\beta\mu$. The
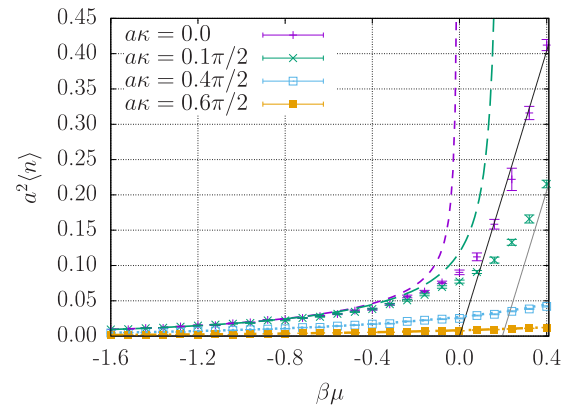

FIG. 4. Average total density, in units of the spatial lattice spacing a, for different values of $a\kappa$ as a function of $\beta\mu$ at $\lambda/a = 0.5$. We also show the noninteracting results for SOC of $\kappa = 0$ (short dashes), $a\kappa = 0.1\pi/2$ (long dashes), $a\kappa = 0.4\pi/2$ (dotted), and $a\kappa = 0.6\pi/2$ (dash-dotted). The continuous lines indicate the mean-field result at $\kappa = 0$ (darker) and $a\kappa = 0.1\pi/2$ (lighter).
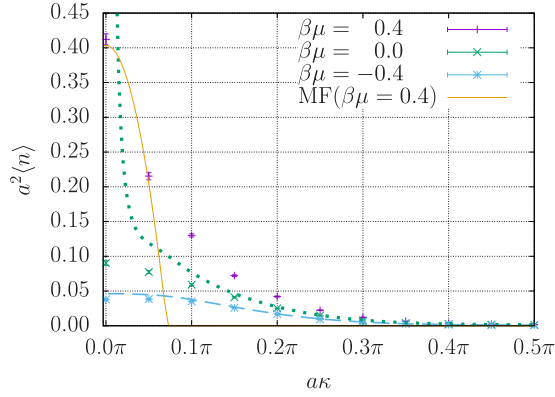
FIG. 5. Average total density, in units of the spatial lattice spacing a, as a function of $a\kappa$ at $\lambda/a = 0.5$. The solid line indicates the mean-field result at $\beta\mu = 0.4$, while the dashed line and dotted lines show the noninteracting results for $\beta\mu = -0.4$ and $\beta\mu = 0.0$, respectively.

mean-field average density for $a\kappa = 0.4\pi/2$ and $0.6\pi/2$ is very small for the chemical potentials considered and not shown on the figure. It is clear that the average density is not well described by the mean-field result for $\mu \leqslant 0$ and/or $\kappa > 0$.

In order to have a better look at the effect of the SOC over the bosonic system, we show in Fig. 5 how the average density changes as we vary κ. For comparison, we also show the mean-field density at $\beta\mu = 0.4$ and noninteracting results at $\beta\mu = -0.4$ and $\beta\mu = 0.0$. In all cases, an increase in the spin-orbit coupling has led to decreasing average densities as the system gets closer to the Weyl-like state.

We have also calculated the pressure difference from a reference value via the Gibbs-Duhem relation

$$P(\mu) - P(\mu_0) = \int_{\mu_0}^{\mu} \langle n(\mu') \rangle d\mu'. \tag{22}$$

The numerical integration has been carried out using the trapezoid rule, with $\beta\mu_0 = -1.6$ as a reference point. We have estimated the errors via bootstrapping with 1000 samples. The results are shown in Fig. 6. The pressure difference in the plot
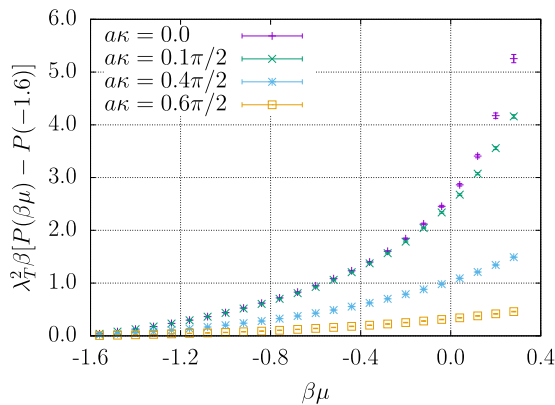

FIG. 6. Pressure difference as a function of $\beta\mu$ for different spin-orbit couplings $a\kappa$. We have used the pressure at $\beta\mu_0 = -1.6$ as reference for each SOC, and plotted in units of $(\beta\lambda_T^2)^{-1}$.
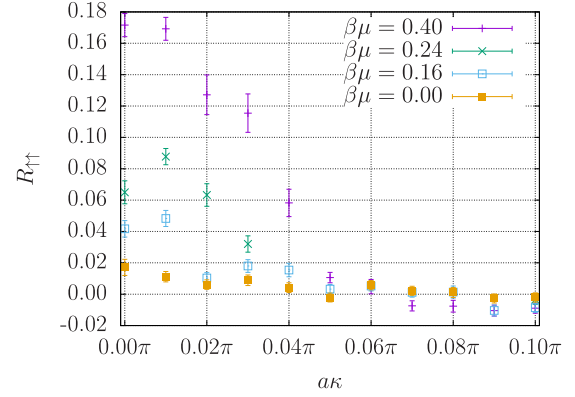

FIG. 7. Pseudocondensate fraction as function of the spin-orbit coupling $a\kappa$ for different chemical potentials $\beta\mu$. The figure shows how the off-diagonal long-range order is destroyed by increasing the SOC.

is shown in units of $1/\beta\lambda_T^2$. One can see that the pressure, as a function of μ and κ, behaves similar to the density, which should be expected from the Gibbs-Duhem relation. As the chemical potential increases, we see an accompanying increase in the pressure, given the larger number of particles within the box. Figure 6 shows that the SOC decreases the density and a similar effect is observed in the pressure, although with lesser intensity.

The confined nature of the simulation volume can induce the formation of (pseudo)condensates at finite temperature. These condensates manifest themselves as off-diagonal long-range order in the correlation function between similar spins. The correlation function is, in general, given by

$$G_{ss'}(|\vec{x} - \vec{y}|) = \langle \phi^{\dagger}_{s(\vec{x}, \tau)} \phi_{s'(\vec{y}, \tau)} \rangle. \tag{23}$$

We show, in Fig. 7, the condensate fraction,

$$R_{ss'} = \frac{G_{ss'}(aN_x/2)}{G_{ss'}(0)}, \tag{24}$$

between two pseudospin "up" fields, as a function of κ and different values of $\beta\mu$. A similar result is obtained for two "down" spins. At $\kappa = 0$ we observe a finite condensate fraction, which tends to zero as κ increases, and is larger for higher values of $\beta\mu$. Beyond $a\kappa > 0.1\pi$, our results for R are compatible with zero and thus excluded from the plot. The correlations between fields of different spins have been measured to be statistically compatible with zero for all values of κ and μ considered.

The above results indicate a destructive interplay between the spin-orbit coupling and condensation in finite systems in two spatial dimensions. A similar phenomenon has been observed in three dimensions with an interspecies coupling in [18] and isotropic s-wave coupling [53].

C. Interacting case II—anisotropic SOC

We have investigated the effects of anisotropic spin-orbit coupling, i.e., $\kappa_x \neq \kappa_y$, on the density equation of state by using $\kappa_y = \eta_{\text{soc}}\kappa_x$, with $0 \leqslant \eta_{\text{soc}} \leqslant 1$. Because of the symmetry $\kappa_x \leftrightarrow \kappa_y$ in the partition function there is no need to consider $\eta_{\text{soc}} > 1$.
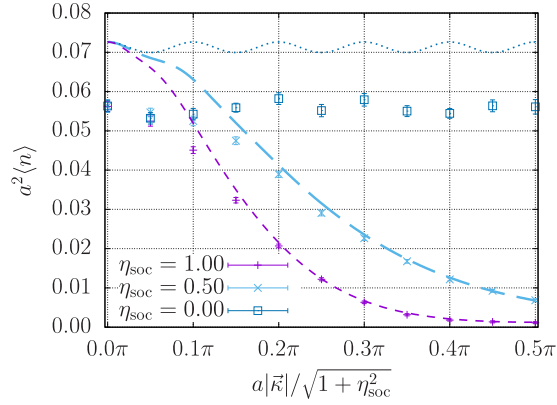
FIG. 8. Average number density, in units of the spatial lattice spacing a, as function of the absolute value of the spin-orbit-coupling vector for $\beta\mu = -0.2$. The lines display the results for the noninteracting case of $\lambda = 0$: short dashes show $\eta_{\text{soc}} = 1.0$, long dashes stand for $\eta_{\text{soc}} = 0.5$, and the dotted line represents $\eta_{\text{soc}} = 0.0$.

In Fig. 8 we plot the average density as function of $|\vec{\kappa}|$. The x axis has been normalized so that the maximum value of $|\vec{\kappa}|$ is the same for all anisotropies. We observe a slower decay of $\langle n \rangle$ as a function of $|\vec{\kappa}|$ for $\eta_{\text{soc}} < 1$. We remind the reader that the mean-field densities for negative chemical potentials are zero. At $\eta_{\text{soc}} = 0.0$ there is a periodic behavior of period $2\pi/N_x$ on the average density for both noninteracting and interacting cases. In the former, we have verified it to be a property of the partition function as a whole, and not of the eigenvalues. Some remnant of this periodicity can be seen at $\eta_{\text{soc}} = 0.5$ for small values of $|\vec{\kappa}|$.

The density equation of state for different SOC anisotropies is shown in Fig. 9 for both interacting (points) and noninteracting (lines) cases. We have used $a\kappa_x = 0.25\pi/2$. Mean-field results are very small in comparison to those in the figure and therefore omitted. The figure shows that the distinction between the interacting and noninteracting equation of states becomes more
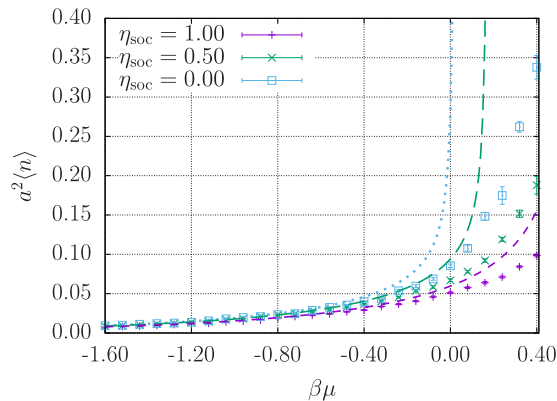

FIG. 9. Density equation of state, in units of the spatial lattice spacing a, for anisotropic spin-orbit couplings at $a\kappa_x = 0.25\pi/2$ and $\lambda/a = 0.5$. Also shown are the noninteracting results for $\eta_{\text{soc}} = 1.0$ (short dashed line), $\eta_{\text{soc}} = 0.5$ (long dashed line), and $\eta_{\text{soc}} = 0.0$ (dotted line). Mean-field results are very small and were omitted.
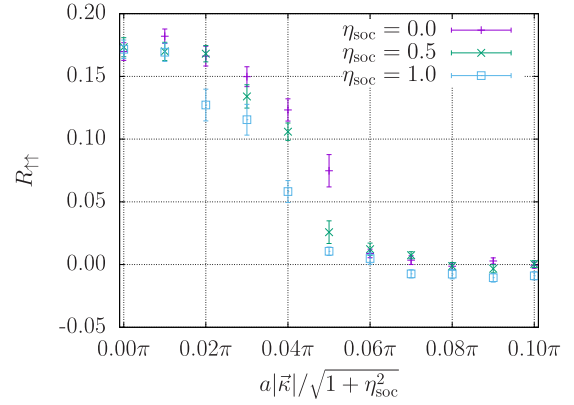

FIG. 10. Plot of the pseudocondensate fraction as function of the absolute value of the spin-orbit-coupling magnitude, for different SOC anisotropies at $\beta\mu = 0.4$. The off-diagonal long-range order survives longer for smaller values of η_{soc}.

pronounced as η_{soc} decreases, and is stronger for larger chemical potentials.

As with the isotropic spin-orbit case, we have investigated the condensate fractions for $\eta_{\text{soc}} < 1$. Figure 10 shows the results for $R_{\uparrow\uparrow}$ as a function of $|\vec{\kappa}|$. Similar to the $\eta_{\text{soc}} = 1$ case, $R_{\downarrow\downarrow}$ displayed a similar behavior. We observe a slower decay of both of the (pseudo)condensate fractions for larger SOC anisotropies. This effect has been seen in three dimensions in [54].

V. SUMMARY AND OUTLOOK

We have investigated the effects of an artificial spin-orbit coupling on the density equation of state for a bosonic system of two pseudospins, as well as contact interactions between similar boson species using nonperturbative numerical methods. The action is complex in Euclidean space-time due to the first-order time derivative, and therefore our method of choice for the simulations was the complex Langevin technique.

Due to how the spin-orbit term enters the lattice formulation, it was possible to investigate how the equation of state changes in the range $0 \leqslant \kappa_x, \kappa_y < \infty$. In particular, the Hamiltonian becomes Weyl-like when the spin-orbit coupling is much larger than the momentum.

We have obtained the density and pressure equations of state for different values of the spin-orbit coupling in the isotropic case, where $\kappa_x = \kappa_y \equiv \kappa$. The average number density has been seen to be a decreasing function of κ, having its minimum value when $a\kappa = \pi/2$ (which corresponds to $\kappa \to \infty$ in the continuum). A comparison with mean-field results has shown that quantum effects play a bigger role for larger values of κ and positive chemical potentials. For $\mu \leqslant 0$ the mean-field average density is zero, in clear contrast with the simulations, which include all quantum effects.

We have also investigated the case of anisotropic spin-orbit coupling, with $\kappa_y = \eta_{\text{soc}}\kappa_x$. A periodic behavior of the number density as a function of the spin-orbit coupling, induced by the finite volume, has been observed in both interacting and noninteracting cases when the SOC anisotropy $\eta_{\text{soc}} = 0$. As η_{soc} is increased from zero towards 1, the aforementioned decaying behavior of the density is recovered.

For both isotropic and anisotropic spin-orbit couplings, we have carried out comparisons between the interacting and noninteracting equations of state. The distinction between them is smallest for large SOC, and becomes more apparent as $|\vec{\kappa}| \rightarrow 0$. Moreover, the finite volume of the simulations allows for the formation of a pseudocondensate, which is depleted by the spin-orbit coupling.

Our investigations have shown that physical pictures based on mean-field results break down in this system. Comparisons with results in three spatial dimensions show similar behavior, despite the differences to that case, in particular how each of them renormalizes.

The effects of spin-orbit coupling over the bosons is very noticeable in the density equation of state: as the SOC increases, the gas becomes more dilute. We have also observed that, even at chemical potentials large enough to support the formation of a pseudocondensate, the presence of the spin-orbit interaction increases the average interparticle distance, such that the pseudocondensates cannot form.

Possible future studies include nonperturbative investigations of the interplay between the spin-orbit coupling and rotation, as well as different types of SOC [55]. Moreover, the determination of physical quantities such as the scattering length or binding energy, which help with connecting with experimental results, can be done via Lüscher's method [56] or the second virial coefficient [57].

APPENDIX: DISCRETIZATION OF THE ACTION

Since the spin-orbit interaction in this case enters the action in the same way as a background gauge field, we shall consider the lattice discretization of a SU(2) gauge theory and then specialize for the SOC. Moreover, we will consider one-dimensional fields, as the generalization to higher dimensions is straightforward. This derivation follows those in [21,22].

The kinetic term for a two component field in the continuum reads

$$K = \Phi^{\dagger}(x)(-i\partial_{\hat{i}})^2 \Phi(x), \tag{A1}$$

where $\hat{i}$ represents a unit vector in the x direction and a is the lattice spacing. Upon discretization, it becomes

$$K_{\text{lat}} = -\frac{\Phi_x^{\dagger}\Phi_{x+a\hat{i}} + \Phi_x^{\dagger}\Phi_{x-a\hat{i}} - 2\Phi_x^{\dagger}\Phi_x}{a^2}. \tag{A2}$$

After applying a local gauge transformation, $\Omega_x \in$ SU(2), the fields become

$$\Phi_{x \pm a\hat{i}} \rightarrow \Omega_{x \pm a\hat{i}} \Phi_{x \pm a\hat{i}},$$
$$\Phi_x^{\dagger} \rightarrow \Phi_x^{\dagger}\Omega_x^{\dagger}, \tag{A3}$$

and the gauge-transformed kinetic term is now

$$K_{\text{lat}} = -\frac{\Phi_x^{\dagger}\Omega_x^{\dagger}\Omega_{x+a\hat{i}}\Phi_{x+a\hat{i}} + \Phi_x^{\dagger}\Omega_x^{\dagger}\Omega_{x-a\hat{i}}\Phi_{x-a\hat{i}} - 2\Phi_x^{\dagger}\Phi_x}{a^2}. \tag{A4}$$

In order to preserve gauge invariance, the derivative must be modified such that

$$\Phi_x^{\dagger}\Phi_{x+a\hat{i}} \rightarrow \Phi_x^{\dagger}U_{x,\hat{i}}\Phi_{x+a\hat{i}},$$
$$\Phi_x^{\dagger}\Phi_{x-a\hat{i}} \rightarrow \Phi_x^{\dagger}U_{x-a\hat{i},\hat{i}}^{\dagger}\Phi_{x-a\hat{i}}, \tag{A5}$$

where the new field U transforms as

$$U_{x,\hat{i}} \rightarrow \Omega_x U_{x,\hat{i}}\Omega_{x+a\hat{i}}^{\dagger}. \tag{A6}$$

By having $U_{x,\hat{i}} = \exp[iaA_{x,\hat{i}}]$, where $A_{x,\hat{i}}$ is the discretized version of the continuum gauge field $A_i(x) \in$ su(2), we have the connection between continuum and lattice versions of the covariant derivatives. Finally, choosing $A_i(x) = \kappa_i \sigma_i$ gives the spin-orbit coupling of Eqs. (2) and (4).

[1] Y.-J. Lin, K. Jiménez-García, and I. B. Spielman, Nature (London) **471**, 83 (2011).

[2] P. Wang, Z. Q. Yu, Z. Fu, J. Miao, L. Huang, S. Chai, H. Zhai, and J. Zhang, Phys. Rev. Lett. **109**, 095301 (2012).

[3] L. W. Cheuk, A. T. Sommer, Z. Hadzibabic, T. Yefsah, W. S. Bakr, and M. W. Zwierlein, Phys. Rev. Lett. **109**, 095302 (2012).

[4] Y.-J. Lin, R. L. Compton, K. Jiménez-García, J. V. Porto, and I. B. Spielman, Nature (London) **462**, 628 (2009).

[5] Y.-J. Lin, R. L. Compton, K. Jiménez-García, W. D. Phillips, J. V. Porto, and I. B. Spielman, Nat. Phys. **7**, 531 (2011).

[6] J. Dalibard, F. Gerbier, G. Juzeliunas, and P. Ohberg, Rev. Mod. Phys. **83**, 1523 (2011).

[7] E. Rashba, Sov. Phys.-Solid State **2**, 1109 (1960).

[8] G. Dresselhaus, Phys. Rev. **100**, 580 (1955).

[9] Z. Wu, L. Zhang, W. Sun, X.-T. Xu, B.-Z. Wang, S.-C. Ji et al., Science **354**, 83 (2016).

[10] J. Léonard, A. Morales, P. Zupancic, T. Esslinger, and T. Donner, Nature (London) **543**, 87 (2017).

[11] J.-R. Li, J. Lee, W. Huang, S. Burchesky, B. Shteynas, F. Ç. Top et al., Nature (London) **543**, 91 (2017).

[12] L. Huang, Z. Meng, P. Wang, P. Peng, S.-L. Zhang, L. Chen et al., Nat. Phys. **12**, 540 (2016).

[13] Z. Meng, L. Huang, P. Peng, D. Li, L. Chen, Y. Xu, C. Zhang, P. Wang, and J. Zhang, Phys. Rev. Lett. **117**, 235304 (2016).

[14] L. Liang and P. Törmä, Phys. Rev. A **100**, 023619 (2019).

[15] C. Wang, C. Gao, C.-M. Jian, and H. Zhai, Phys. Rev. Lett. **105**, 160403 (2010).

[16] H. Zhai, Rep. Prog. Phys. **78**, 026001 (2015).

[17] E. Kawasaki and M. Holzmann, Phys. Rev. A **95**, 051601(R) (2017).

[18] R. Liao, Phys. Rev. Lett. **120**, 140403 (2018).

[19] S. Stringari, Phys. Rev. Lett. **118**, 145302 (2017).

[20] P. Mujal, A. Polls, and B. Juliá-Díaz, arXiv:1907.13355.

[21] H. J. Rothe, World Sci. Lect. Notes Phys. **43**, 1 (1992).

[22] C. Gattringer and C. B. Lang, Lect. Notes Phys. **788**, 1 (2010).

[23] P. Hasenfratz and F. Karsch, Phys. Lett. B **125**, 308 (1983).

[24] T. Ozawa and G. Baym, Phys. Rev. A **84**, 043622 (2011).

[25] G. Juzeliūnas, J. Ruseckas, M. Lindberg, L. Santos, and P. Öhberg, Phys. Rev. A **77**, 011802(R) (2008).

[26] A. C. Loheac and J. E. Drut, Phys. Rev. D **95**, 094502 (2017).

[27] A. C. Loheac, J. Braun, and J. E. Drut, Phys. Rev. D **98**, 054507 (2018).

[28] L. Rammelmüller, A. C. Loheac, J. E. Drut, and J. Braun, Phys. Rev. Lett. **121**, 173001 (2018).

[29] L. Rammelmüller, W. J. Porter, J. E. Drut, and J. Braun, Phys. Rev. D **96**, 094506 (2017).

[30] C. E. Berger, L. Rammelmüller, A. C. Loheac, F. Ehmann, J. Braun, and J. E. Drut, arXiv:1907.10183.

[31] D. Sexty, Phys. Lett. B **729**, 108 (2014).

[32] F. Attanasio and B. Jäger, Eur. Phys. J. C **79**, 16 (2019).

[33] J. B. Kogut and D. K. Sinclair, Phys. Rev. D **100**, 054512 (2019).

[34] D. Sexty, Phys. Rev. D **100**, 074503 (2019).

[35] K. Nagata, J. Nishimura, and S. Shimasaki, J. High Energy Phys. 07 (2016) 073.

[36] J. Bloch, J. Glesaaen, J. J. M. Verbaarschot, and S. Zafeiropoulos, J. High Energy Phys. 03 (2018) 015.

[37] T. Hayata and A. Yamamoto, Phys. Rev. A **92**, 043628 (2015).

[38] C. Berger and J. Drut, PoS **LATTICE2018**, 244 (2018).

[39] J. Nishimura and A. Tsuchiya, J. High Energy Phys. 06 (2019) 077.

[40] G. Parisi and Y.-S. Wu, Sci. Sin. **24**, 483 (1981).

[41] G. Aarts, F. A. James, E. Seiler, and I.-O. Stamatescu, Phys. Lett. B **687**, 154 (2010).

[42] G. Parisi, Phys. Lett. B **131**, 393 (1983).

[43] J. R. Klauder, Acta Phys. Austriaca Suppl. **25**, 251 (1983).

[44] J. R. Klauder, J. Phys. A **16**, L317 (1983).

[45] J. R. Klauder, Phys. Rev. A **29**, 2036 (1984).

[46] G. Aarts and I.-O. Stamatescu, J. High Energy Phys. 09 (2008) 018.

[47] G. Aarts, Phys. Rev. Lett. **102**, 131601 (2009).

[48] G. Aarts, E. Seiler, and I.-O. Stamatescu, Phys. Rev. D **81**, 054508 (2010).

[49] G. Aarts, F. A. James, E. Seiler, and I.-O. Stamatescu, Eur. Phys. J. C **71**, 1756 (2011).

[50] M. Scherzer, E. Seiler, D. Sexty, and I.-O. Stamatescu, Phys. Rev. D **99**, 014512 (2019).

[51] M. Scherzer, E. Seiler, D. Sexty, and I. O. Stamatescu, Phys. Rev. D **101**, 014501 (2020).

[52] U. Wolff (ALPHA Collaboration), Comput. Phys. Commun. **156**, 143 (2004).

[53] T. Ozawa and G. Baym, Phys. Rev. Lett. **109**, 025301 (2012).

[54] X. Cui and Q. Zhou, Phys. Rev. A **87**, 031604(R) (2013).

[55] T.-L. Ho and S. Zhang, Phys. Rev. Lett. **107**, 150403 (2011).

[56] M. Lüscher, Commun. Math. Phys. **105**, 153 (1986).

[57] C. R. Shill and J. E. Drut, Phys. Rev. A **98**, 053615 (2018).